Article

Influence of Separation Gap on the Performance of Savonius Hydrokinetic Turbine

Mafira Ayu Ramdhani, Arun George and Il Hyoung Cho *

Department of Ocean System Engineering, Jeju National University, Jeju 63243, Korea;
mafiraramdhani@gmail.com (M.A.R.); arunmvgorge@gmail.com (A.G.)

* Corresponding author. E-mail: cho0904@jejunu.ac.kr (I.H.C.)

ABSTRACT: Despite that ocean current energy is one of the promising sources of electricity produced in the ocean, the development of ocean current energy is far behind compared to other ocean energy due to the low efficiency and high cost of installation and maintenance. Among many converting devices, the Savonius turbine has been proven to be effective and competitive in harnessing ocean current energy. The primary purpose of the present study is to search for the optimum shape of a Savonius rotor based on CFD simulation (Star-CCM+). A Savonius turbine composed of two rotating cup-shaped rotors is selected as a numerical model. We focus on the effect of two geometry parameters such as the overlap and gap ratio on the power coefficient. Throughout the parametric study, the shape of a Savonius rotor affects the power performance, and two geometry parameters with an overlap ratio of 0.15 and a gap ratio of −0.03 are found to be the optimum design. It demonstrates stable performance within the wide TSR (Tip Speed Ratio) range of 0.6 to 1.6, with the maximum power coefficient C_p of 0.34 achieved at a TSR of 0.8. According to the numerical results based on the new CFD model, the presence of a bottom wall does not significantly affect the performance of a Savonius turbine. It means that the present unbounded CFD model can be acceptable in the initial design stage for the determination of the geometry parameters of a Savonius turbine.

1. Introduction

In the modern days, electricity has become an indispensable element of daily life. However, a significant portion of electricity is still generated from fossil fuels such as coal, oil, and gas, giving rise to serious environmental problems like global warming, which in turn leads to severe floods and droughts worldwide [1]. Therefore, to prevent the earth from being hotter, governments and researchers must develop renewable clean energy as an alternative to fossil fuels. Solar, hydropower, wind, biomass, geothermal, and ocean energy belong to renewable and clean energy. The electricity produced from hydropower, solar, wind, and geothermal are currently used in several countries. But, despite the potential of ocean energy, challenges remain in the research and development of efficient energy converting devices, assessment of environmental impact, and establishment of policies and regulations. Even though the commercialization of ocean energy is way slower compared to other renewable energy sources, ocean energy will allow millions of homes to be powered soon [2].

Ocean energy exists in the forms of wind, wave, ocean/tidal current, and thermal and salinity gradients. It is estimated that this potential ranges from 20,000 to 80,000 terawatt-hours (TWh) of electricity annually, which is 100–400% of current global demand. Ocean energy development lags significantly in technical maturity when compared to other renewable sources like onshore wind and solar. However, as has been demonstrated in the case of the development of onshore wind and solar energy, the difficulty of ocean energy development will be overcome. Also, economic feasibility will be greatly increased by investment, innovation, and installation of prototypes. Recently, most of the researchers focused on ocean/tidal current energy owing to uniformity. As a conversion system from the kinetic energy inherent in water movement to mechanical energy, a variety of turbines connected to the generator are essentially used. The hydrokinetic turbine suitable for ocean/tidal current converter must be designed considering the following: initial

installation cost, maintenance fee, efficiency, and working even at low-velocity conditions. Turbines may be classified as horizontal-axis turbines (HATs) and vertical-axis turbines (VATs) [3]. When considering the installation site, an appropriate type of turbine need to be selected.

A Savonius rotor rotates due to the drag force exerted by the moving fluid. These crossflow systems are not highly efficient, primarily because the difference in the drag forces between the two curved surfaces is available to turn the rotor. The concave surface captures the moving fluid, inducing more drag than the convex surface. Even though a Savonius rotor shows low efficiency, it has the advantage that it can self-start in low-speed flow conditions [4]. Efficiency has been improved further by using more elaborate developed design tools, recently. Regarding the Savonius rotor, much research has been conducted to improve its performance, such as the aspect ratio (AR) [5,6], overlap ratio (OR) [6,7], number of blades [5,8,9], blade shape, addition of end plate, and rotor angle. Although studies on the Savonius rotor working in water are scarce, they show that the hydrokinetic Savonius rotor can produce greater energy than the aerodynamic Savonius rotor [10].

Nakajima et al. (2008) tested the environmentally sustainable Savonius hydraulic turbine. They evaluated the effect of two parameters such as the clearance ratio and rotation direction of the Savonius rotor. Here the clearance ratio means the gap distance between the rotor and the bottom surface divided by a turbine diameter. According to their research, a turbine shows the best performance when a turbine rotates counterclockwise, and the clearance ratio is greater than 0.73. They showed that the variation of the flow field around the rotor due to the clearance ratio affected its performance [11].

In addition, the adjustment of the separation gap between two rotors can have a significant impact on the rotor's performance. This separation gap accelerated the fluid flow from the concave side of the advancing rotor to the returning rotor, thereby reducing negative torque. The separation gap can be subdivided by two key parameters, such as the overlap ratio and gap ratio. According to the related studies, it was reported that the optimum overlap ratio was within the range of 0.15–0.30 [12]. Most studies focused mainly on the overlap ratio, on the other hand, the effect of the gap ratio on the efficiency of the Savonius rotor was not reported much.

Ushiyama and Nagai (1988) conducted experiments on a conventional Savonius wind turbine with two cup-shaped rotors with five different gap ratios. They observed that the gap ratio of −0.05 yielded the best performance among them. Also, it was found that an increase in the gap ratio between the two rotors led to a decrease in the torque coefficient throughout intensive experiments. They recommended that it is advisable to give a small negative gap ratio to the Savonius rotor [13].

Kerikous and Thevenin (2019) carried out the numerical calculations using Star-CCM++ and in-house optimization code (OPAL++) was used to search for the optimum overlap ratio (OR) and gap ratio (GR) on the Savonius hydrokinetic turbine. Within a variation range of OR and GR from 0 to 0.42, the optimum range of OR is between 0.12–0.21, and the optimum GR is around 0.033 [14]. Their study only focused on the positive gap ratio. Hence, the negative gap ratio on a Savonius hydrokinetic turbine is still in the veil and requires additional research.

The present study assesses the performance of the Savonius hydrokinetic rotor by investigating the power coefficient in the combination of overlap ratio and gap ratio, including positive and negative gap ratio. The computational fluid dynamics (CFD) simulation was conducted with an unbounded model, in which symmetric conditions at the top and bottom boundary are imposed. It helps to reduce the simulation time, but the influence of the adjacent boundaries such as the bottom wall and free surface on the turbine's performance need to be investigated. Therefore, a new CFD model with a non-slip condition at the bottom wall is examined to verify the effect of the bottom wall on the performance of a Savonius turbine. The SST k-ω turbulent mode with Reynolds-Averaged Navier-Stokes (RANS) formulations is employed for CFD simulation. The Savonius turbine consists of two cup-shaped rotors. Notably, the present study focuses on the comprehensive investigation of the effect of a variety of overlap ratios and gap ratios on the hydrodynamic performance of the Savonius turbine in uniform flow. The present paper is organized into four sections. Section 2 presents the key design parameters affecting the power of a Savonius rotor. Section 3 demonstrates the mesh generation and the computational domain setup. Section 4 shows the validation of the present CFD model through the comparison of Nakajima's experiment, and the detailed results and discussion on the effects of the overlap ratio and gap ratio on the hydrodynamic performance of a Savonius rotor. Section 5 summarizes the main conclusions drawn from the present study.

2. Savonius Rotor

In the ocean current with speed U, the power across a cross-sectional area (A) can be expressed by the following equation.

$$P_I = \frac{1}{2}\rho A U^3 \tag{1}$$

where ρ is the sea water density (=1024 kg/m³).

A fraction of the ocean energy that passes through the energy conversion system can be extracted [14] for electricity. This ratio of the extracted power to input power is called as power coefficient, C_P, and can be expressed as:

$$C_P = \frac{P_E}{P_I} = \frac{P_E}{0.5\rho A U^3} \tag{2}$$

where P_E which is the mechanical power extracted through the conversion system is expressed by:

$$P_E = Q\omega = \frac{2\pi NQ}{60} \tag{3}$$

where Q is the torque (Nm) and ω the angular velocity of a rotor, and N is the revolution-per-minute (RPM).

The power coefficient is closely dependent on the tip speed ratio (TSR), which is defined by the ratio of the speed of the tips of the rotor to the undisturbed current speed U. Given a rotor radius of R, the TSR (λ) can be expressed as:

$$\lambda = \frac{\omega R}{U} \tag{4}$$

Besides the power coefficient, the torque coefficient (C_t) is also an important parameter in determining the performance of the Savonius rotor:

$$C_t = \frac{Q}{Q_I} = \frac{Q}{0.5\rho A U^2 R} \tag{5}$$

The numerical rotor model as shown in Figure 1 is the same as an experimental model adopted by Nakajima et al. [11]. The specification of a rotor model is listed in Table 1.

Two key parameters affecting the rotor's performance are the overlap ratio and the gap ratio (Figure 2). The overlap ratio (OR) is defined as the ratio of the overlap distance (e) to the diameter (D_B) of a rotor as follows:
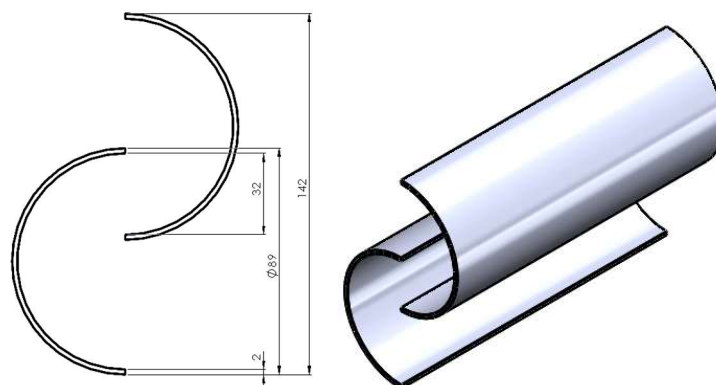
$$OR = \frac{e}{D_B} \tag{6}$$

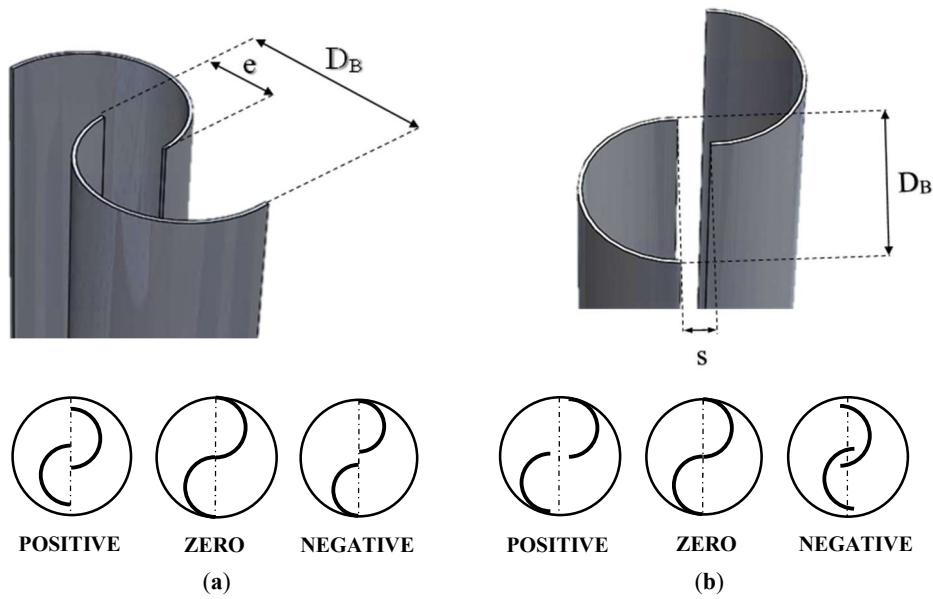On the other hand, the gap ratio (GR) is the ratio of the gap distance (s) to the diameter of a rotor.

$$GR = \frac{s}{D_B} \tag{7}$$

Table 1. Turbine dimensions.

Parameter	Specifications
Turbine length (L_R)	210 mm
Turbine diameter (D_R)	142 mm
Aspect ratio (AR = L_R/D_R)	1.48
Number of rotors	2
Rotor diameter (D_B)	89 mm
Rotor thickness (de)	2 mm

Figure 1. Numerical model of a Savonius turbine with two rotors.

Figure 2. Schematic sketch of a Savonius turbine with (**a**) overlap ratio and (**b**) gap ratio.

3. Numerical Calculation

3.1. Computational Domain

For simplicity, the present numerical model is assumed to be a 2D model rather than a 3D model, therefore, the Savonius turbine is assumed to be infinitely long along the *y*-axis. In this study, a finite volume method (FVM), which is a well-established computational approach widely used in the field of fluid dynamics, has been employed. This method is utilized to discretize the fluid domain and solve the governing equations within the discretized numerical domain. To accurately capture the movement of the Savonius rotor, we have employed the overset mesh technique for faster convergence and superior accuracy when compared to the sliding mesh technique, as documented in previous research [15,16]. To implement the overset mesh technique, the entire fluid domain is divided into two distinct sub-domains: a rotating domain, which rotates together with the rotor, and a stationary domain which represents the flow of water [17]. The overset mesh domain positioned between them plays a crucial role in facilitating the seamless transfer of mesh data between the rotating and stationary domains. It is worth noting that our numerical simulations are conducted in an unsteady state, allowing us to capture the rate of dynamic changes over time.

The fluid domain is 2.556 m (18D) in length and 1.704 m (12D) in height. The rotor is positioned at 6D from the inlet and symmetry wall. The size of the overset domain is 0.1704 m (1.2D), 20% larger than the rotor diameter. At the inlet boundary, a uniform current velocity is prescribed, while a uniform pressure condition is considered at the outlet boundary. The top and bottom boundaries are treated as symmetry conditions, signifying that the rotor is situated within an unbounded fluid domain. In addition, a no-slip condition, which is enforced along the surface of the rotor, is applied to the bottom boundary to investigate the effect of the bottom wall on the performance of a turbine. For a visual representation of the computational domain and boundary conditions, please refer to Figure 3.
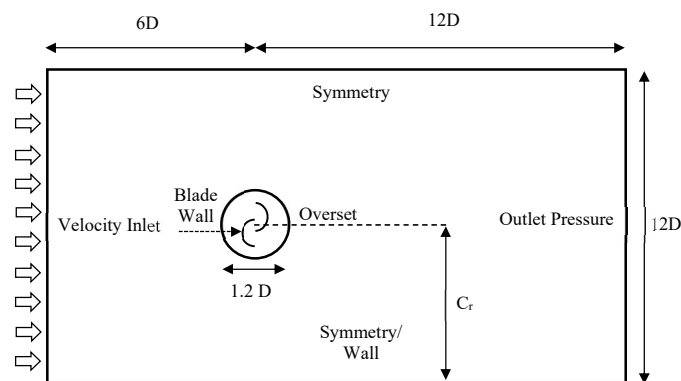

**Figure 3.** Computational domain and boundary condition.

3.2. Mesh Generation

The process of mesh generation is a pivotal stage when conducting efficient and precise CFD calculations for a given numerical model, as emphasized in previous studies [17]. A high-quality mesh is imperative for obtaining accurate, stable, and convergent numerical solutions [18]. Therefore, it is needed to assess the adequacy of mesh resolution prior to commencing a numerical simulation. In the present CFD simulation, we have employed a 2D automated mesh generation approach utilizing a polygonal meshing model. Specifically, we have incorporated 20 prism layer cells around the rotor. This strategic placement of prism layer cells helps to enhance the resolution of the boundary layer, contributing to the overall accuracy of the simulation.

Furthermore, to optimize the distribution of meshes, we have chosen to employ finer cell sizes within the rotating domain, which encompasses the rotor itself, in comparison to the stationary domain. The mesh sizing in three different numerical domains (rotating, overset, stationary) around the rotor is depicted in Figure 4, demonstrating the difference in mesh distribution in each domain. Searching for the optimum number of meshes, the mesh convergence test is conducted by evaluating the coefficient of power of the rotor for seven different numbers of cells, varying from coarse to very fine mesh including the different prism layers configuration. As shown in Figure 5, when considering CPU time, storage, and accuracy comprehensively, the number of meshes of 1.8×10^5 seems to be an appropriate value. This number of cells is employed in the afterward calculations.
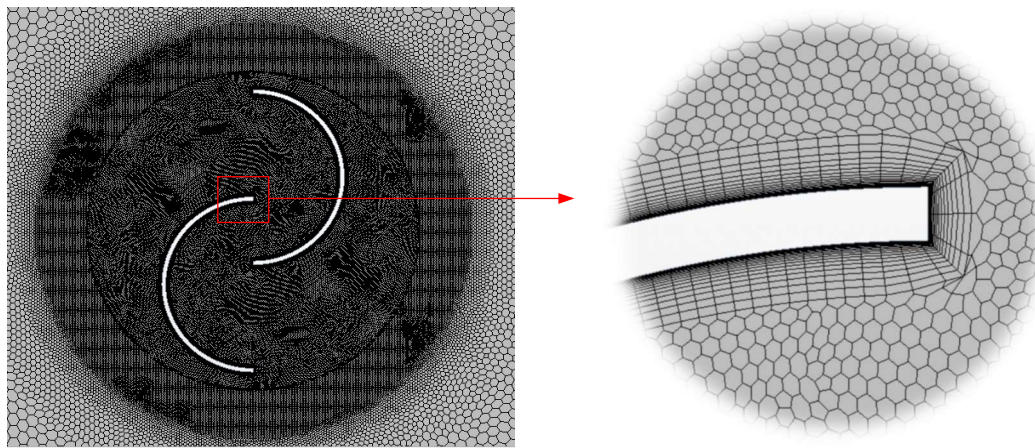
Figure 4. Mesh distribution in three different numerical domains.
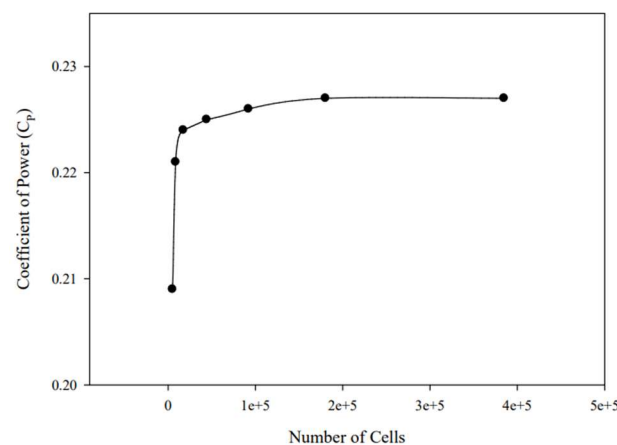
Figure 5. Mesh convergence test on a Savonius with OR of 0.36 and GR of 0 at TSR 1.0.

3.3. Solver Setting

In CFD simulation, we adopted the Reynolds-Averaged Navier-Stokes (RANS) turbulence models. The preference for the RANS models over Large Eddy Simulation (LES) is attributed to the latter's high computational cost. The shear stress transport (SST) k-ω model [14,19] is the combined model of the k-ω model and the k-ε model. The former shows merit within the boundary layer near walls, while the latter advantage for free stream flow beyond the boundary layers. Further, the SST k-ω turbulence model has merits for its good behavior in adverse pressure gradients and separating flow. Thus, the SST k-ω model exhibits exceptional computational efficacy in the horizontal and vertical axis hydrokinetic

turbines [20–22]. A second-order upwind scheme is applied for time discretization. In addition, to perform a faster and more efficient time-marching simulation, the maximum time step size is selected to be 0.004 s by the criterion that the rotating angle is not over 1 degree in each time step. In the rotating domain, a non-dimensional wall distance (y+) value is kept below 1 by managing the distance of the first prism layer on the rotor wall.

4. Result and Discussion

4.1. Numerical Validation

To confirm the model's reliability, the numerical results are compared with Nakajima's experimental data for clockwise rotation at the clearance ratio of 1.08 and overlap ratio of 0.36. The detailed information on the material and properties of the Savonius rotor model was referred to [11]. The average power coefficient (C_P) is used for the comparison with the experiments. In Figure 6, the average power coefficient shows a good agreement within the overall range TSR [0.6, 1.6]. The slight discrepancy between numerical and experimental results at some TSR values is attributed to the flow separation occurring at high angular speed where the SST k-ω turbulence model shows its limitation. As the present numerical model is proven to be reliable, the present numerical model will be used to perform the parametric study for the optimum shape of a Savonius rotor.
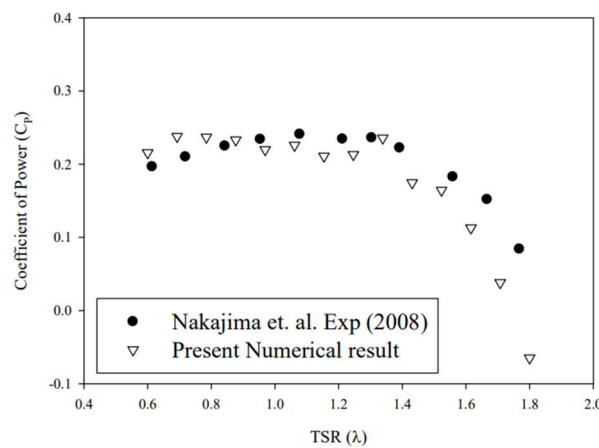
Figure 6. Comparison between the present numerical results and Nakajima et al. [11] experimental results at different TSR.

4.2. Effect of Overlap Ratio

In this section, we examine how the overlap ratio affects the performance of a Savonius rotor. The overlap ratios are selected to be 0.15, 0.20, 0.25, 0.30, and 0.36 in the numerical calculation, where Nakajima's experimental model among them belongs to 0.36. A rotor's average torque and power are obtained from the time-series data in unsteady simulation, and then the torque coefficient and power coefficient are calculated. Figure 7 depicts the torque and power coefficient as a function of TSR and overlap ratio. Observing Figure 7a, it is evident that the torque coefficient exhibits a general trend of consistent decline as the TSR increases. On the other hand, the power coefficient shows a distinct pattern that exists a peak value within the TSR range of [0.6, 0.8] and decreases with increasing TSR.
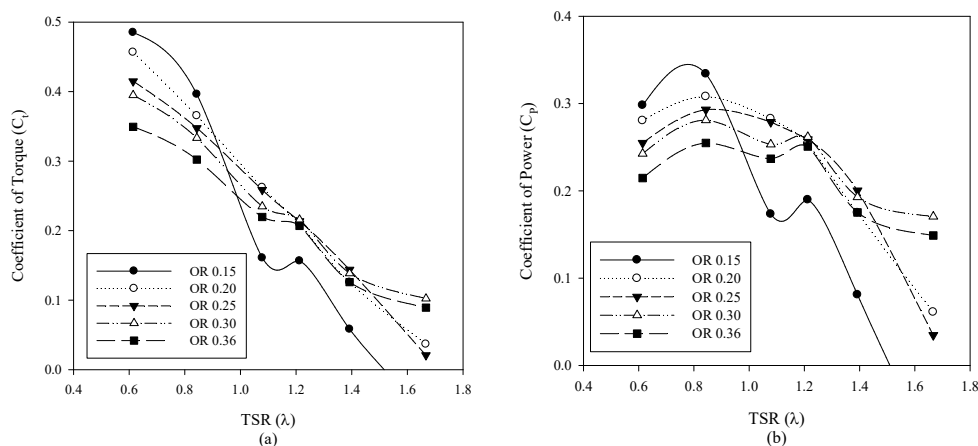
Figure 7. Influence of overlap ratio as a function of TSR on (**a**) toque coefficient and (**b**) power coefficient at a zero gap ratio.

The Savonius turbine with an overlap ratio of 0.15 provides the maximum peak value of the power coefficient at TSR = 0.8. However, when TSR is beyond 0.8, the power coefficient shows a rapid decrease. Similar results of performance degradation with the increase of TSR have been reported by Akwa et al. [23] for the two-bucket Savonius wind rotor with the semi-circular shape. It is worth noting that the Savonius turbine with the other overlap ratios except the overlap ratio of 0.15 maintains a relatively wide peak width across the TSR range.

4.3. Effect of Gap Ratio

Let us investigate how the gap ratio affects the performance of a Savonius rotor. The gap ratios used in the calculation are −0.05, −0.03, 0.0, 0.03, and 0.05 with a fixed overlap ratio of 0.36. In Figure 8, the torque and power coefficients are shown as a function of TSR and the gap ratio.

In comparison with the overlap ratio shown in Figure 7, it is apparent that the torque and power coefficients are unaffected significantly by the gap ratio within the low TSR range of [0.6, 1.2]. In the low TSR range, the power coefficient gives a slightly higher value at the gap ratio having a minus value than a positive gap ratio. However, the power coefficient for gap ratios of −0.05 and −0.03 experiences a sharp decrease when TSR exceeds 1.2. The positive gap ratios of 0.03 and 0.05 consistently maintain high power coefficient values at larger TSR values. From this perspective, it can be concluded that the Savonius rotor achieves its optimum performance at a gap ratio of 0.03. Similar findings are also reported by Kerikous and Thevenin [14], with the optimum value of the gap ratio being 0.033.
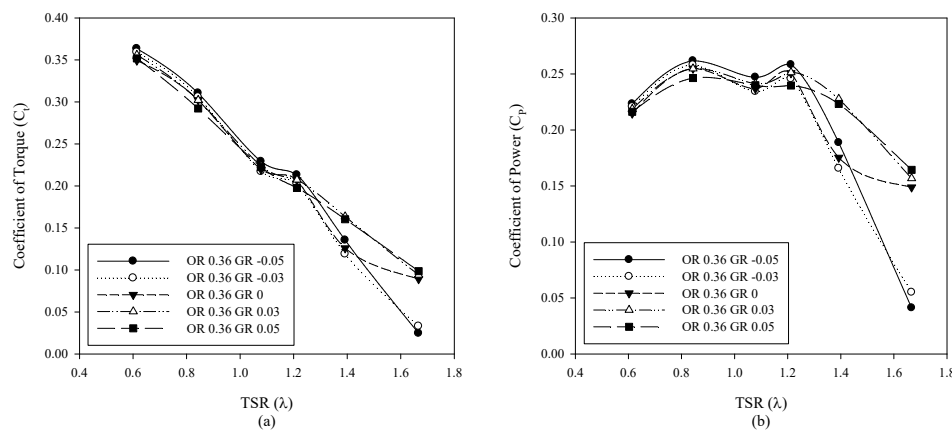

Figure 8. Influence of gap ratio as a function of TSR on (**a**) torque coefficient and (**b**) power coefficient at a fixed overlap ratio of 0.36.

In the next figure, numerical calculations were conducted on positive gap ratios with zero overlap ratio to gain a comprehensive understanding of the gap ratio's impact on the Savonius rotor. As shown in Figure 9, the torque coefficient decreases with increasing TSR for five different positive gap ratios (0.01, 0.03, 0.05, 0.07, and 0.1). However, it exhibits a sudden plunge at TSR of 1.0, then rises gradually with the increase of TSR. The power coefficients show comparatively higher values at TSR of less than 0.9 for all gap ratios, they have a minimum value at TSR of 1.0, and then increase monotonously with TSR. Notably, the Savonius rotor with a gap ratio of 0.03 at the TSR of 0.9 achieved the highest power coefficient, reaching 0.276.
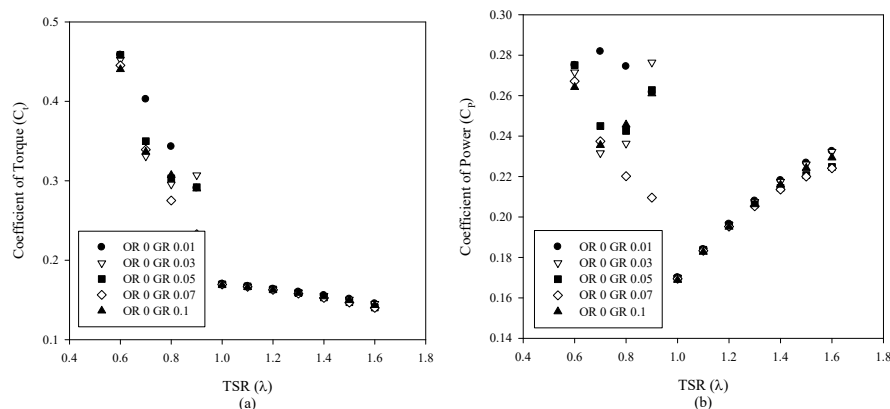
Figure 9. Influence of positive gap ratio as a function of TSR on the (**a**) torque coefficient and (**b**) power coefficient at a zero overlap ratio.

A comparison of velocity vectors between gap ratios of 0.03 and 0.1 at TSR of 0.9 and zero overlap ratio is presented in Figure 10. The vorticity patterns downstream exhibit slight differences with two gap ratios. Specifically, the larger and more unbalanced wake vorticities are observed at a gap ratio of 0.1, and the strong vorticities appear closer to the rotor tip. Consequently, the power extraction performance of a larger gap ratio (=0.1) can be estimated to be slightly less than that of the smaller gap ratio (=0.03) due to the energy dissipation caused by vorticity generation.

(**a**) GR = 0.03

(**b**) GR = 0.1
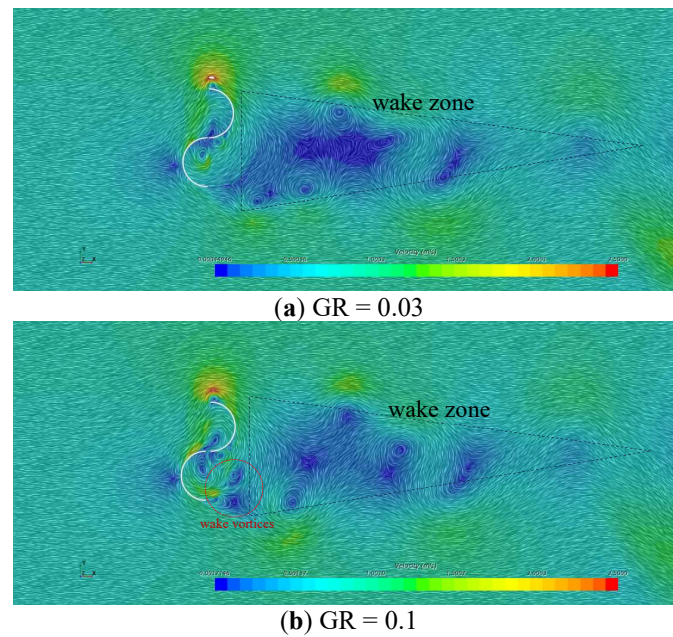
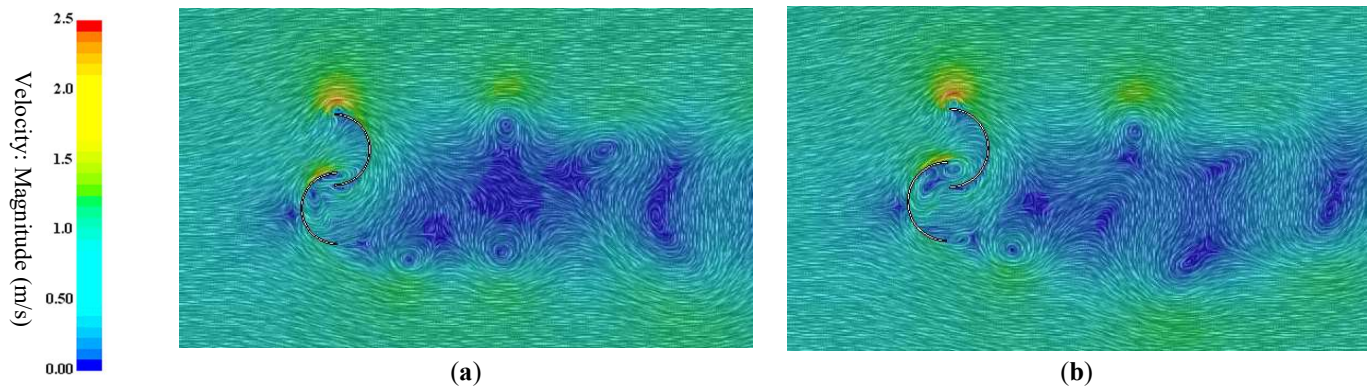**Figure 10.** Velocity vector visualization around rotors for two different gap ratios at a TSR of 0.9.

4.4. Combination Effect of Overlap and Gap Ratio

In the previous sections, we conducted independent assessments of the influence of both overlap ratio and gap ratio on the performance of a Savonius turbine. In this section, we perform a comprehensive investigation of the combined effects of two parameters. Eight combinations are taken from overlap ratios of 0.15, 0.2, 0.25, 0.3, and gap ratios of 0.03 and −0.03. From a design perspective, our findings suggest that the most favorable separation ratio lies between these two parameters. In Figure 11, within the TSR range from 0.9 to 1.0, it is observed that the combination of an overlap ratio of 0.15 and a gap ratio of −0.03, as well as an overlap ratio of 0.20 and a gap ratio of −0.03, yields the highest power coefficient. However, it is noted that the combination representing the highest power coefficient decreases its performance suddenly as TSR increases. Notably, a Savonius turbine with an overlap ratio of 0.20 and a gap ratio of −0.03 can extract a maximum power coefficient of 0.34 when operating at a TSR of 1.0. On the other hand, the combination of an overlap ratio of 0.15 with gap ratios of 0.03 s provides a more stable and wider operating range with high performance, offering favorable characteristics for certain applications.
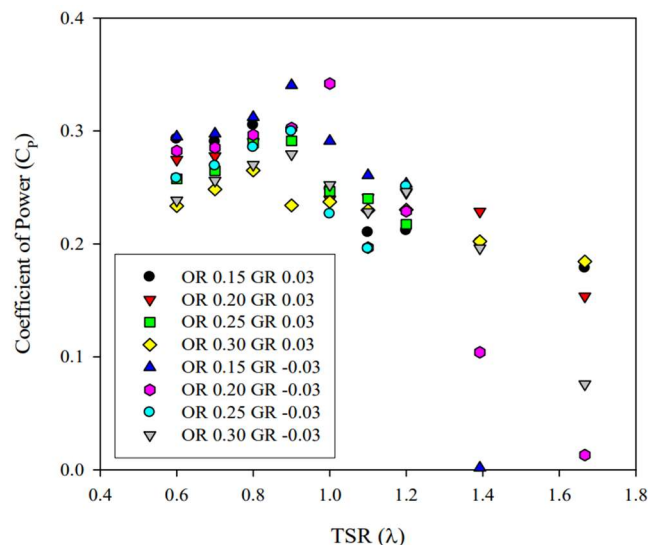
Figure 11. Influence of the overlap and gap ratios as a function of TSR on the power coefficient.

Figure 12. Velocity vector visualization around rotors for (**a**) OR 0.15, GR −0.03 (**b**) OR 0.3, GR 0.03 at a fixed TSR of 0.9.

Another velocity vector plot is drawn in Figure 12 to examine the effect of the separation ratio on the flow field around a turbine. Two different combinations with the overlap ratio and gap ratio of (0.15, −0.03) and (0.3,0.03) are selected. At a fixed TSR of 0.9, the Savonius turbine with a combination of (0.15, −0.03) gave the maximum power coefficient in Figure 11, whereas the combination of (0.3, 0.03) belongs to the lowest power coefficient. When comparing two velocity vectors, it is observed that the vorticity in a wake zone behind a turbine shows a different pattern from each other. A combination of (0.15, −0.03) shows that smaller and clearer vorticities are formed, and the number of vorticities is much. In the combination of (0.3, 0.03), the neighboring vorticities are merged, and the larger vorticities are formed and shed downstream. As a result, more vigorous turbulent flow in the wake zone is produced. Also, the recirculation vortex that existed between the rotor gap encourages momentum loss and contributes to a decrease in the power coefficient.

In Figure 13, the power coefficients are compared for three different combinations of the overlap and gap ratio including conventional Savonius turbine with zero gap ratio. Talukdar et al. [24] conducted experiments on a vertical Savonius (VATs) model with an overlap ratio of 0.15 and zero gap ratio. Their experimental data are used for the comparison of CFD results for the turbines with the combination of overlap ratio and gap ratio. Figure 13 demonstrates how the turbine performance is affected significantly by the sign of gap ratio. Within the range of 0.6–1.2 of TSR, a Savonius turbine with a negative gap ratio produces more power than the turbine with a positive gap ratio and with zero gap ratio. The maximum power coefficient is 0.34 at a TSR of 0.9. However, despite the comparatively reduced value of peak, the turbine with a positive gap ratio maintains without a sudden drop of the power coefficient across the entire TSR range.
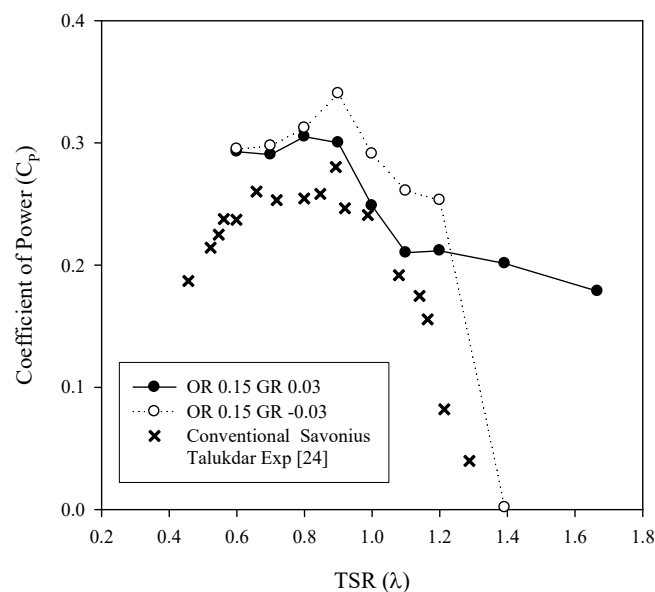

Figure 13. Comparison of the power coefficient between three different combinations of the overlap and gap ratio.

4.5. Effect of Bottom Wall Condition

In this study, the Savonius turbine is assumed to be positioned in an unbounded fluid domain by imposing symmetric conditions at the top and bottom boundaries. Although this assumption contributes to help reducing the huge CPU time for finding the optimal values of the gap and overlap ratio, the systematic investigation of the influence of the bottom wall and free surface is necessary for the practical applications of the Savonius turbine. The symmetric condition at the bottom is replaced with a no-slip condition but the symmetric condition at the top is maintained. The effect of the free surface at the top will be left for the next research. The scenario for bottom wall effect was dependent on the distance between the center of turbine and the bottom wall defined as C_r. In Figure 14, we compared the power coefficient of a Savonius turbine for three different gap distances (C_r/D_R = 0.8, 1.7, 3.0) at the fixed overlap ratio of 0.15 and gap ratio of −0.03.

We expect the performance of a Savonius turbine can be affected by the bottom wall, which varies the flow patterns and flow velocity around the rotor. Figure 14 shows that the intermediate gap distance with C_r/D_R of 1.7 gives a maximum power coefficient in the region less than TSR = 1.0, but the presence of the bottom wall is not significant in comparison with the unbounded fluid model. These results mean that the unbounded CFD model can be acceptable in the initial design stage of a Savonius turbine.
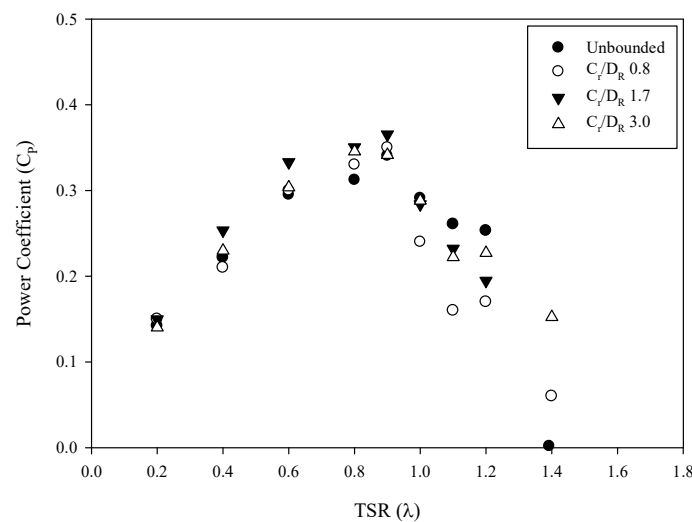
Figure 14. Comparison of Savonius performance on the influence of bottom effect.

5. Conclusions

In this study, we performed a comprehensive parameter study on the shape of a Savonius rotor, focusing on nondimensional parameters such as gap ratio and overlap ratio. From this investigation, several key conclusions have been drawn:

1. The findings obtained from CFD simulations show the Savonius rotor with an overlap ratio of 0.15 achieves a peak efficiency of 0.334 at a TSR of 0.8, while an overlap ratio of 0.3 exhibits stable behavior across the TSR range of 0.6 to 1.6.
2. Regarding the gap ratio, the negative gap ratio demonstrates slightly higher power coefficients at a lower TSR range showing a sudden drop in a high range of TSR, whereas the positive gap ratio provides a wider operational range without a sudden decline.
3. The separation gap (gap ratio and overlap ratio) of a Savonius rotor affects the patterns of wake vorticity downstream behind the rotor and the rotor tip vortex. The performance of a Savonius rotor depends on the characteristics of these vortices, which cause unfavorable energy dissipation.
4. From the parametric study with two parameters such as the gap and overlap ratio, a Savonius rotor with an overlap ratio of 0.15 and a gap ratio of −0.03 is proved to be an optimum shape. A Savonius rotor designed from this combination demonstrates stable performance within the wide TSR range of 0.6 to 1.6, together with a highest power coefficient of 0.34 achieved at a TSR of 0.8.
5. The effect of the bottom wall on the performance of a Savonius turbine is also investigated. The maximum power coefficient is achieved at Cr/DR of 1.7 in the low TSR region less than 1.0. However, the bottom wall with different gap distances follows the trend of an unbounded model, without significant quantitative difference. It indicates clearly that the unbounded CFD model is acceptable in the preliminary design stage.

Declaration of Competing Interest

The authors declare that they have no known competing financial interests or personal relationships that could have appeared to influence the work reported in this paper.

References

1. Hannah R, Max R, Pablo R. Energy. Published online at OurWorldInData.org. 2022. Available online: https://ourworldindata.org/energy (accessed on 4 March 2023).
2. De Andres A, MacGillivray A, Roberts O, Guanche R, Jeffrey H. Beyond LCOE: a study of ocean energy technology development and deployment attractiveness. *Sustain. Energy Tech.* **2017**, *19*, 1–16.
3. Sheng Q, Jing F, Zhang L, Zhou N, Wang S, Zhang Z. Study of the hydrodynamic derivatives of vertical-axis tidal current turbines in surge motion. *Renew. Energy* **2016**, *96*, 366–376.
4. Satrio D, Utama IKAP, Mukhtasor. Vertical axis tidal current turbine: Advantages and challenges review. 2016; pp. 64–71. Available online: http://isomase.org/OMAse/Vol.3-2016/Section1/3-7.pdf (accessed on 2 March 2023).
5. Zhao Z, Zheng Y, Xu X, Liu W, Hu G. Research on the improvement of the performance of Savonius rotor based on numerical study. In Proceedings of the 2009 International Conference on Sustainable Power Generation and Supply, Nanjing, China, 6–7 April 2009.
6. Kamoji MA, Kedare SB, Prabhu SV. Performance tests on helical Savonius rotors. *Renew. Energy* **2009**, *34*, 521–529.
7. Gupta R, Biswas A, Sharma KK. Comparative study of a three-bucket Savonius rotor with a combined three-bucket Savonius–three-bladed Darrieus rotor. *Renew. Energy* **2008**, *33*, 1974–1981.
8. Satrio D, Muhammad FY, Mukhtasor, Rahmawati S, Junianto S, Musabikha S. Numerical simulation of crossflow Savonius turbine for locations with low current velocity in Indonesia. *J. Braz. Soc. Mech. Sci. Eng.* **2022**, *44*, 315.
9. Saha UK, Thotla S, Maity D. Optimum design configuration of Savonius rotor through wind tunnel experiments. *J. Wind Eng. Ind. Aerodyn.* **2008**, *96*, 1359–1375.
10. Sarma NK, Biswas A, Misra RD. Experimental and computational evaluation of Savonius hydrokinetic turbine for low velocity condition with comparison to Savonius wind turbine at the same input power. *Energy Conv. Manag.* **2014**, *83*, 88–98.
11. Nakajima M, Iio S, Ikeda T. Performance of Savonius rotor for environmentally friendly hydraulic turbine. *J. Fluid Sci. Tech.* **2008**, *3*, 420–429.
12. Maldar NR, Ng CY, Oguz E. A review of the optimization studies for Savonius turbine considering hydrokinetic applications. *Energy Conv. Manag.* **2020**, *226*, 113495.
13. Ushiyama I, Nagai H. Optimum design configurations and performance of Savonius rotors. *Wind Eng.* **1988**, *12*, 59–75.
14. Kerikous E, Thévenin D. Performance enhancement of a hydraulic Savonius turbine by optimizing overlap and gap ratios. In Proceedings of the ASME 2019 Gas Turbine India Conference, Chennai, India, 5–6 December 2019.
15. Nichols R, Tramel R. Applications of a highly efficient numerical method for overset mesh moving body problems. In Proceedings of the 15th Applied Aerodynamics Conference, Atlanta, GA, USA, 23–25 June 1997.
16. Lopez Mejia OD, Mejia OE, Escorcia KM, Suarez F, Laín S. Comparison of sliding and overset mesh techniques in the simulation of a vertical axis turbine for hydrokinetic applications. *Processes* **2021**, *9*, 1933.

17. Boissonnat JD, Cohen-Steiner D, Mourrain B, Rote G, Vegter G. Meshing of Surfaces. In *Effective Computational Geometry for Curves and Surfaces*; Springer: Berlin/Heidelberg, Germany, 2007; pp. 181–230.
18. UniAET. *Simcenter STAR-CCM+ Basic Training*; Siemens: Munich, Germany, 2020.
19. Chaudhari VN, Shah SP. Numerical Investigation of Savonius Hydrokinetic Turbine Having Novel Thick Blades. *J. Phys. Conf. Ser.* **2023**, *2629*, 012012.
20. López O, Meneses D, Quintero B, Laín S. Computational study of transient flow around Darrieus type cross flow water turbines. *J. Renew. Sustain. Energy* **2016**, *8*, 014501.
21. Menter FR, Kuntz M, Langtry R. Ten years of industrial experience with the SST turbulence model. *Turbul. Heat Mass Transf.* **2003**, *4*, 625–632.
22. Amet E, Maître T, Pellone C, Achard JL. 2D numerical simulations of blade-vortex interaction in a Darrieus turbine. *J. Fluids Eng.* **2009**, *131*, 111103.
23. Akwa JV, da Silva Júnior GA, Petry AP. Discussion on the verification of the overlap ratio influence on performance coefficients of a Savonius wind rotor using computational fluid dynamics. *Renew. Energy* **2012**, *38*, 141–149.
24. Talukdar PK, Sardar A, Kulkarni V, Saha UK. Parametric analysis of model Savonius hydrokinetic turbines through experimental and computational investigations. *Energy Conv. Manag.* **2018**, *158*, 36–49.